Supplementary Information

Active-layer thickness prediction and regional differences across permafrost regions using a physics-residual machine-learning workflow

Seungwon Baek[1], Seung Hee Kim[2], Yoon Taek Jung[2], Yongchae Cho[1,*]

[1]Seoul National University, Department of Energy Systems Engineering, Seoul, 08826, Republic of Korea
[2]Korea Polar Research Institute, Center of Remote Sensing and GIS, Incheon, 21990, Republic of Korea
*Corresponding author: yc.cho@snu.ac.kr

This file contains Supplementary Methods, Supplementary Tables S1–S7 and Supplementary Figures S1–S12.

Supplementary Methods

Label processing and units

A site-year is one observation location (coordinates rounded to 0.0001°) in one observation year, and a cell-year is the mean over the sites in one 1 km map cell in one year (Supplementary Table S5). ABoVE version 2 [1] contains 529,862 thaw-depth records. Restricting the records to 45–80°N, to measurements of August–October and to ALT values greater than 0 and less than 300 cm left 223,937 records, and 4824 measurements of January–July were excluded as early-season values. ABoVE records the instrument of each measurement. The instruments are probes (uncertainty 3 cm) and GPR. A GPR value is the two-way travel time converted to depth with the wave velocity determined at probe calibration points measured every few minutes along the transect (median reported uncertainty 8.3 cm). Of the Alaska site-years, 10,880 (70%) are GPR values, 2517 are probe measurements, 1532 have no instrument recorded and 611 are CALM grid means. The GPR transects lie in 13 of the Alaska blocks and make up 96% of the 2014 site-years. All Canadian ABoVE site-years (1131) are probe measurements. CALM [2] provides 1673 site-years in Alaska and Canada. Of these, 189 could not be matched to a cell of the covariate table and were excluded, and the remaining 1484 were merged by site location into 1426 site-years. Of the 9186 ALLena [3] records, the 6827 values of August–September without the probe-limit flag were used, and the seasonal maximum per location and year gave 3282 site-years. Of all 20,768 site-years, 19,172 fall in 2010–2024, the years with year-specific climate input. Multiple measurements at a site in one year were averaged, and the mean observation day was kept for the accumulation of thawing degree-days (TDD).

Climate variables

All climate variables were computed from the monthly ERA5-Land means of the observation year of each site-year. TDD is the sum of the positive monthly mean air temperatures multiplied by the number of days in each month, and the value at the observation day was obtained by linear interpolation of the cumulative TDD to the end of each month in the day of year. The freezing degree-days and the mean temperature of the coldest month were computed for the winter preceding the thaw season (October of the previous year to April of the observation year). The snow water equivalent is the mean of the hydrological year ending in the observation year (October of the previous year to September). The soil temperature is the annual mean of the top ERA5-Land soil layer (0–7 cm). For cells classified as sea in ERA5-Land, the value of the nearest land grid cell within 0.2°, and then within 0.5°, was used. The mean climate input in Fig. 3a of the main text is the 2011–2024 mean of the yearly values (2010 is excluded because its winter variables are incomplete). All other analyses used the input of the observation year, and the yearly maps used the input of the map year with the TDD accumulated to 1 September.

Products: extraction, coverage and training data

All six products are openly available (licences in Supplementary Table S1). The products of Wei et al. [4], Liu et al. [5], ESA CCI [6, 7] and Aalto et al. [8] cover the entire Northern Hemisphere permafrost region and are intended for use also in regions without training data. The product of Yi and Kimball [9] covers only Alaska. For the yearly products, the value of the observation year was extracted at the cell centre. Values were read from the 1 km EPSG:3995 rasters for Wei et al., from the 1/120° rasters for Liu et al., from the yearly NetCDF files for ESA CCI v4 and v5, and from the Alaska NetCDF file for Yi and Kimball. Aalto et al. provide one value for 2000–2014. Version 2 of the Wei et al. product was trained on 2196 annual observations of 2000–2020 at 201 CALM and GTN-P sites, and the site coordinates are published. The median distance from the label cells to the nearest training site is 7 km in Alaska, 107 km in the Lena Delta and 222 km in Canada (Supplementary Fig. S6). The product of Liu et al. was trained on 2966 site-years from CALM, an earlier version of the ABoVE data (2008–2020), ABCflux and sites on the Tibetan Plateau. ESA CCI is a process model driven by remotely sensed land-surface temperature and is not trained on ALT observations. The mean product bias by latitude band (prediction minus observation) was computed on the label site-years with a product value for the observation year.

Product-anchored residual learning and SHAP

In the product-anchored test, the product value p of the observation year was recalibrated on the training fold as $a+bp$ (least squares), and the residual learner of the main model was trained on $y-(a+bp)$ with the same 23 inputs and $\lambda = 0.5$. The folds were the spatial-block folds of the main analysis, and only site-years with a product value were evaluated. SHAP values [10] were computed with the exact tree algorithm of CatBoost for the residual model ($y-\hat{y}_P$) and the direct model trained on all labels of each region, and they were summarised as mean absolute values per variable and per variable group.

Sensitivity analyses

Three sensitivity analyses were carried out to complement the main results. (i) Weight of the residual correction (Supplementary Table S4). At $\lambda = 0.25$, 0.5 and 1, the RMSE difference from the recalibrated Stefan model under spatial-block cross-validation was −2.0, −3.6 and −5.1 cm in the Lena Delta, −2.0, −3.7 and −6.3 cm in Canada and −0.2, −0.2 and +0.3 cm in Alaska. Under region hold-out, the difference from the source-coefficient Stefan model was +0.8, +2.0 and +5.4 cm in the Lena Delta. As λ increased, both the within-region gain and the error in the withheld region increased. At all three values, the physics-residual model was more accurate than direct ML in the withheld Lena Delta and Alaska. Its RMSE was also within 6.8, 3.3 and 5.4 cm of the most accurate of the three methods (recalibrated Stefan model, physics-residual model and direct ML) in all 15 combinations of region and validation design (direct ML 17.8 cm, recalibrated Stefan model 10.8 cm). (ii) Alaska without the 2014 survey. The difference in spatial-block RMSE between the full-season year-specific input and the 2011–2024 mean input was 0.0 [−0.7, +0.9] cm for the physics-residual model and +0.8 [−0.2, +1.8] cm for the recalibrated Stefan model. Without the 2014 labels, the effect of the year-specific input in Alaska still could not be distinguished from zero. (iii) Alaska without the GPR values (4660 site-years in 72 blocks; models retrained). The spatial-block RMSE was 23.7 cm for the recalibrated Stefan model, 24.0 cm for the physics-residual model (+0.3 [−0.4, +0.6] cm) and 25.1 cm for direct ML (+1.4 [−1.3, +2.8] cm). The difference between the year-specific and the mean input for the physics-residual model was −1.1 [−1.7, +0.2] cm. When the region hold-out results of the main analysis were scored on the same site-years, the RMSEs of the source-coefficient Stefan model, the physics-residual model and direct ML were 24.0, 24.4 and 25.7 cm, respectively. The small difference between the physics-residual model and the recalibrated Stefan model, and the absence of an advantage of direct ML in the withheld Alaska, were therefore the same with and without the GPR values. In the main analysis, the GPR site-years had a smaller error than the probe site-years (physics-residual model 15.3 versus 26.1 cm), and the GPR values also had a smaller spread (standard deviation 16.3 versus 28.1 cm).

Computing environment

The CatBoost experiments (validation designs, covariate sets, label-number and transfer experiments, product-anchored test and SHAP) were run on a 96-core CPU node, and the neural learners (MLP, TabM and FT-Transformer) on one NVIDIA A100 GPU. The software used was Python 3.9, CatBoost 1.2.10, PyTorch 2.6, scikit-learn 1.3 and NumPy 1.26. All training used fixed random seeds, and the predictions of three seeds were averaged in each experiment before scoring.

Table S1. Data sources, versions, licences and repositories.

Data	Version, identifier	Licence	Repository
ABoVE soil moisture and ALT [1]	v2, https://doi.org/10.3334/ORNLDAAC/2369	NASA EOSDIS open	ORNL DAAC
ALLena thaw depth [3]	https://doi.org/10.1594/PANGAEA.973813	CC BY 4.0	PANGAEA
GTN-P CALM [2]	https://doi.org/10.1594/PANGAEA.972777	CC BY 4.0	PANGAEA
ERA5-Land monthly means [11, 12]	reanalysis-era5-land-monthly-means	Copernicus licence	Climate Data Store
Copernicus DEM [13]	GLO-30, https://doi.org/10.5270/ESA-c5d3d65	Copernicus DEM licence	AWS Open Data
SoilGrids 2.0 [14]	250 m	CC BY 4.0	ISRIC
MODIS [15, 16]	MOD13Q1, MOD10A2 v6.1	NASA EOSDIS open	AppEEARS
Global Surface Water [17]	v1.4 (1984–2021), occurrence	Copernicus, free of charge	JRC, Google
NCSCD [18, 19]	v2, 0.012° raster	open, citation requested	Bolin Centre
Raster CAVM [20]	https://doi.org/10.17632/c4xj5rv6kv.2	CC BY-NC 3.0	Mendeley Data
ESA WorldCover [21]	2021 v200, https://doi.org/10.5281/zenodo.7254221	CC BY 4.0	AWS Open Data
ESA CCI permafrost probability and ALT v4 [6, 22]	v4.0	ESA CCI data policy	CEDA
ESA CCI ALT v5 [7]	v5.0	ESA CCI data policy	CEDA
Wei et al. [4, 23]	https://doi.org/10.5281/zenodo.21667583 (v2)	CC BY 4.0	Zenodo
Liu et al. [5, 24]	https://doi.org/10.5281/zenodo.10070610	CC BY 4.0	Zenodo
Aalto et al. [8, 25]	https://doi.org/10.5061/dryad.886pr72	CC0	Dryad
Yi and Kimball [9]	https://doi.org/10.3334/ORNLDAAC/1760	NASA EOSDIS open	ORNL DAAC

Table S2. Input variables. The main model uses the first three groups (23 variables).

Group	Variables	Source, resolution	Time
Climate (8)	mean annual air temperature; TDD; $\sqrt{\text{TDD}}$; warmest monthly mean temperature; freezing degree-days and coldest monthly mean temperature of the preceding winter; annual mean soil temperature at 0–7 cm; snow water equivalent of the preceding hydrological year	ERA5-Land, 0.1°	observation year
Terrain (6)	elevation; slope; sine and cosine of aspect; topographic position index; roughness (33 × 33 window)	Copernicus DEM, 30 m	static
Soil (9)	clay, sand, silt, bulk density, coarse fragments, pH (5–15 cm); soil organic carbon 0–5, 5–15, 15–30 cm	SoilGrids 2.0, 250 m	static
MODIS (sensitivity)	summer NDVI and EVI (June–August); snow-off day; snow days	MOD13Q1 250 m, MOD10A2 500 m	observation year
High resolution (sensitivity)	NCSCD soil organic carbon [18, 19]; CAVM class [20]; WorldCover fractions [21]	1 km and finer	static
Lagged climate (sensitivity)	TDD, freezing degree-days and snow water equivalent of the previous year	ERA5-Land	year before the observation

Table S3. Labels, climate inputs and products used in each analysis.

Analysis (display item)	Labels	Climate input	Products
Year-specific against mean input (Fig. 3a)	all site-years 2010–2024	observation year to the observation day; 2011–2024 mean	–
Validation designs (Fig. 3b, c; Supplementary Table S4)	all site-years	observation year to the observation day	–
Covariate sets and terciles (Fig. 4a, b)	all site-years	as above; MODIS of the observation year	–
Label number within a region (Supplementary Fig. S5)	random draws from the training folds	as above	–
Transfer with target labels (Fig. 4c)	other two regions, plus target draws	as above	–
Common site-years (Fig. 5; Supplementary Table S6)	2010–2020 (Alaska 2010–2020, Lena Delta 2013–2020, Canada 2010–2019)	as above	Wei et al., Liu et al., CCI v4 of the same year
RMSE per observation year (Supplementary Fig. S7)	years with ≥30 site-years	as above	Wei et al. to 2024, Liu et al. to 2020
Cell-year rescoring (Supplementary Table S5)	as the validation designs, averaged per 1 km cell and year	as above	–
Product maps (Fig. 6)	Alaska and Canada 2013, Lena Delta 2016 (most observed cells)	TDD to 1 September of that year	Wei et al., Liu et al. of the same year
Yearly maps (Fig. 7)	training 2010–2024	TDD to 1 September of each year 2011–2024	–
Product-anchored test (Supplementary Fig. S8)	site-years with a product value	as above	Wei et al. 2010–2024

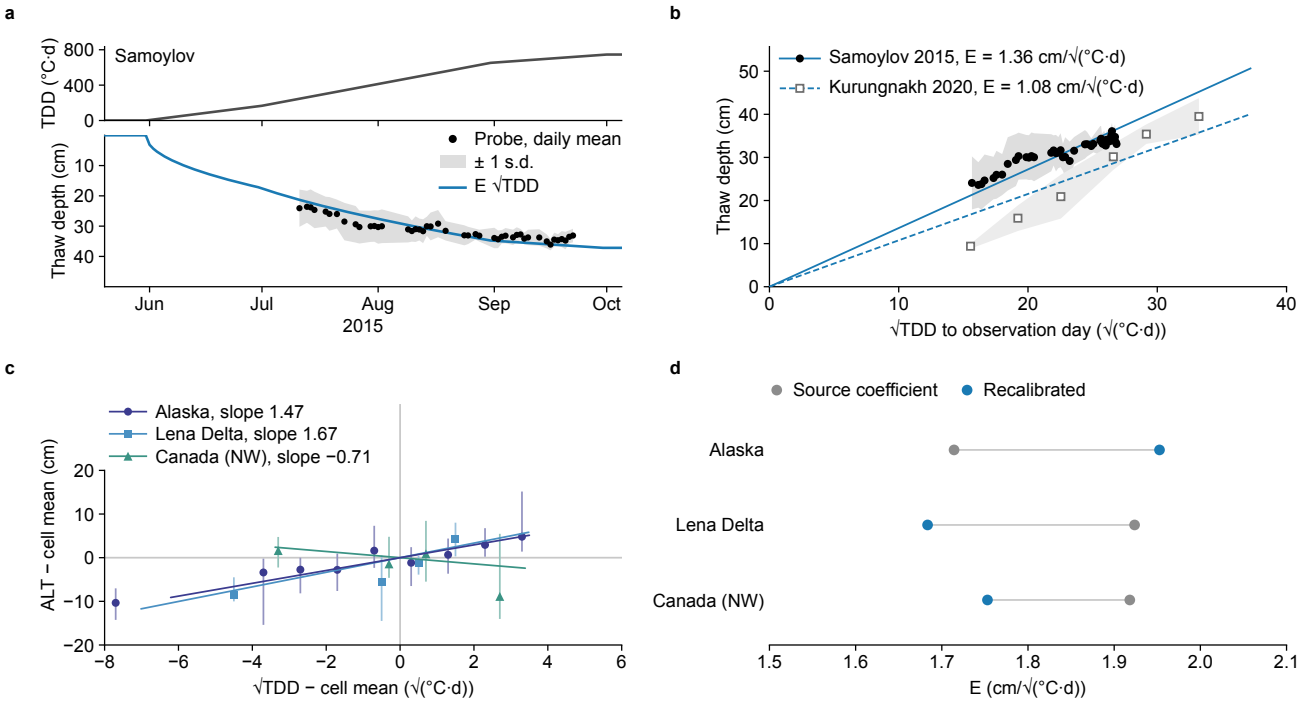

Figure S1. Stefan relation within a season and among years. (a) Cumulative TDD and thaw depth at Samoylov, 2015. (b) Thaw depth against $\sqrt{\text{TDD}}$ at Samoylov and Kurungnakh. (c) Deviations of ALT and $\sqrt{\text{TDD}}$ from the site means at sites observed in four or more years. (d) Stefan coefficient by region.

Table S4. RMSE (cm) of all methods under the five validation designs. λ, weight of the residual correction in equation (5).

Method	Random	Spatial block	Year	Block-year	Region held out
Alaska					
Physics + residual ML ($\lambda = 0.5$)	14.0	18.4	17.3	18.5	17.5
$\lambda = 0.25$	15.9	18.4	17.9	18.5	17.9
$\lambda = 1$	11.8	18.9	16.9	19.0	20.3
Stefan, recalibrated	18.2	18.6	18.7	18.8	19.4
Stefan, source coeff.	19.4	19.4	19.4	19.3	19.4
Kudryavtsev, scaled	21.1	21.7	21.3	21.3	25.1
Direct ML	11.8	17.3	14.8	17.5	20.6
Physics-input ML	11.9	17.5	14.9	17.8	19.6
Physics pseudo-labels	13.0	18.4	17.7	18.7	19.3
Lena Delta					
Physics + residual ML ($\lambda = 0.5$)	14.8	17.4	20.1	20.7	23.5
$\lambda = 0.25$	17.4	19.0	20.6	21.0	22.3
$\lambda = 1$	12.3	16.0	19.6	20.4	26.8
Stefan, recalibrated	20.5	21.0	21.2	21.5	21.5
Stefan, source coeff.	21.5	21.5	21.5	21.6	21.5
Kudryavtsev, scaled	19.8	20.4	20.8	21.0	21.8
Direct ML	12.3	15.9	20.2	20.6	39.3
Physics-input ML	12.2	16.1	19.9	20.8	41.2
Physics pseudo-labels	15.4	20.7	21.1	21.5	21.5
Canada (NW)					
Physics + residual ML ($\lambda = 0.5$)	19.5	26.9	24.3	28.0	24.2
$\lambda = 0.25$	22.9	28.6	25.8	29.4	25.4
$\lambda = 1$	16.2	24.4	23.8	26.2	26.3
Stefan, recalibrated	27.0	30.6	28.1	31.1	27.8
Stefan, source coeff.	27.7	27.7	27.4	26.9	27.8
Kudryavtsev, scaled	24.6	25.4	24.6	24.2	35.4
Direct ML	16.2	26.1	24.6	28.1	23.9
Physics-input ML	16.2	25.6	23.8	27.0	23.5
Physics pseudo-labels	18.8	30.5	27.0	31.0	27.4

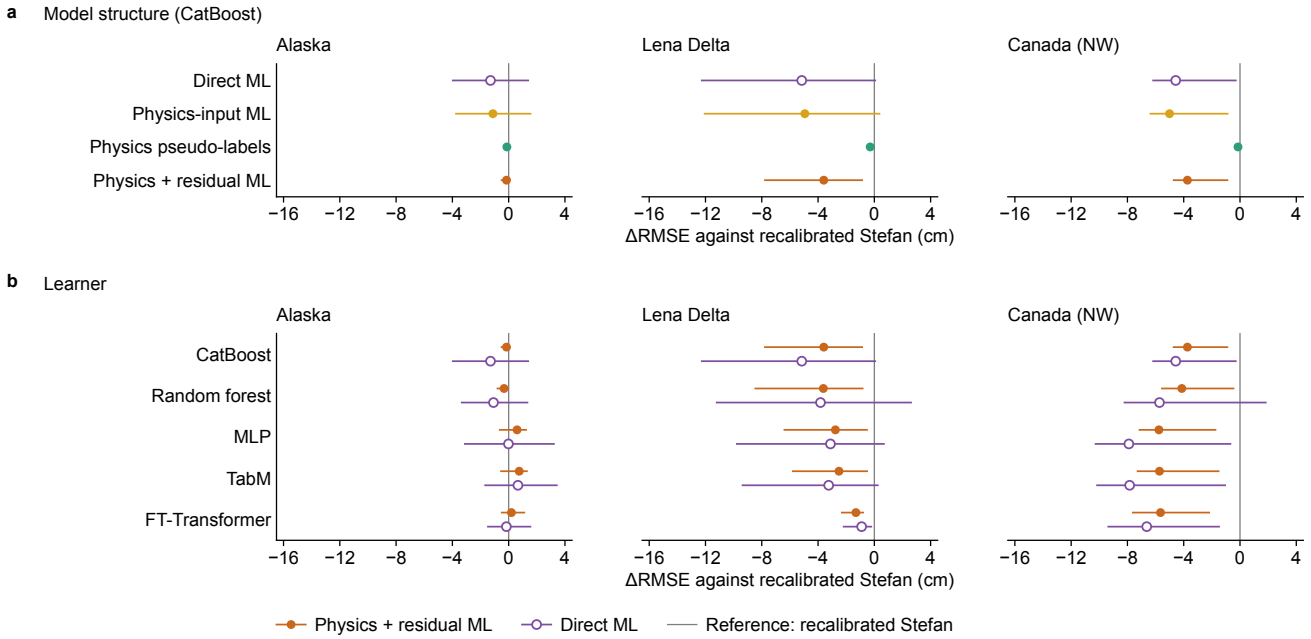

Figure S2. Position of the physical information and choice of learner. Difference in spatial-block RMSE from the recalibrated Stefan model for four model structures (a) and five learners (b). Error bars, 95% block-bootstrap intervals.

Table S5. RMSE on site-years and on 1 km cell-years. (a) RMSE (cm) under three validation designs. (b) Paired differences (cm) with 95% block-bootstrap intervals.

(a)

Region	Design	*n* (site-years / cell-years)	Physics + residual ML	Stefan (recal.)	Stefan (source)	Direct ML
Alaska	Spatial block	15,540 / 910	18.4 / 24.0	18.6 / 24.0	19.4 / 24.3	17.3 / 24.7
Alaska	Region hold-out	15,540 / 910	17.5 / 23.4	19.4 / 24.3	19.4 / 24.3	20.6 / 23.9
Alaska	Random	15,540 / 910	14.0 / 16.2	18.2 / 23.8	19.4 / 24.3	11.8 / 11.2
Lena Delta	Spatial block	2436 / 244	17.4 / 15.6	21.0 / 19.2	21.5 / 19.7	15.9 / 14.6
Lena Delta	Region hold-out	2436 / 244	23.5 / 22.2	21.5 / 19.7	21.5 / 19.7	39.3 / 37.4
Lena Delta	Random	2436 / 244	14.8 / 13.0	20.5 / 19.0	21.5 / 19.7	12.3 / 10.0
Canada (NW)	Spatial block	1196 / 144	26.9 / 31.7	30.6 / 34.2	27.7 / 32.1	26.1 / 29.7
Canada (NW)	Region hold-out	1196 / 144	24.2 / 31.8	27.8 / 32.1	27.8 / 32.1	23.9 / 33.3
Canada (NW)	Random	1196 / 144	19.5 / 20.6	27.0 / 33.7	27.7 / 32.1	16.2 / 13.2

(b)

Region	Design	Comparison	Site-years, ΔRMSE [95% CI]	Cell-years, ΔRMSE [95% CI]
Alaska	Spatial block	Physics + residual ML − Stefan (recalibrated)	−0.2 [−0.6, +0.1]	−0.00 [−1.8, +1.2]
Alaska	Spatial block	Direct ML − Stefan (source coeff.)	−2.1 [−5.4, +1.5]	+0.4 [−2.1, +1.6]
Alaska	Region hold-out	Physics + residual ML − Stefan (source coeff.)	−1.8 [−4.9, +1.0]	−0.9 [−2.3, +0.9]
Alaska	Region hold-out	Direct ML − Stefan (source coeff.)	+1.2 [−1.0, +2.3]	−0.5 [−3.1, +2.9]
Alaska	Random	Direct ML − Stefan (source coeff.)	−7.5 [−9.6, −5.1]	−13.1 [−21.6, −4.7]
Lena Delta	Spatial block	Physics + residual ML − Stefan (recalibrated)	−3.6 [−7.8, −0.8]	−3.6 [−7.3, −0.8]
Lena Delta	Spatial block	Direct ML − Stefan (source coeff.)	−5.6 [−10.3, −1.2]	−5.1 [−9.5, −0.5]
Lena Delta	Region hold-out	Physics + residual ML − Stefan (source coeff.)	+2.0 [−0.8, +3.4]	+2.5 [+0.4, +4.2]
Lena Delta	Region hold-out	Direct ML − Stefan (source coeff.)	+17.8 [+8.0, +23.9]	+17.7 [+12.4, +24.8]
Lena Delta	Random	Direct ML − Stefan (source coeff.)	−9.2 [−16.1, −3.8]	−9.7 [−15.9, −3.7]
Canada (NW)	Spatial block	Physics + residual ML − Stefan (recalibrated)	−3.7 [−4.8, −0.8]	−2.5 [−3.9, −1.4]
Canada (NW)	Spatial block	Direct ML − Stefan (source coeff.)	−1.7 [−4.9, +2.5]	−2.4 [−4.8, −0.3]
Canada (NW)	Region hold-out	Physics + residual ML − Stefan (source coeff.)	−3.5 [−5.1, −0.1]	−0.2 [−2.3, +1.8]
Canada (NW)	Region hold-out	Direct ML − Stefan (source coeff.)	−3.8 [−7.0, +1.4]	+1.2 [−2.2, +4.3]
Canada (NW)	Random	Direct ML − Stefan (source coeff.)	−11.6 [−15.7, −7.2]	−18.9 [−33.3, −6.7]

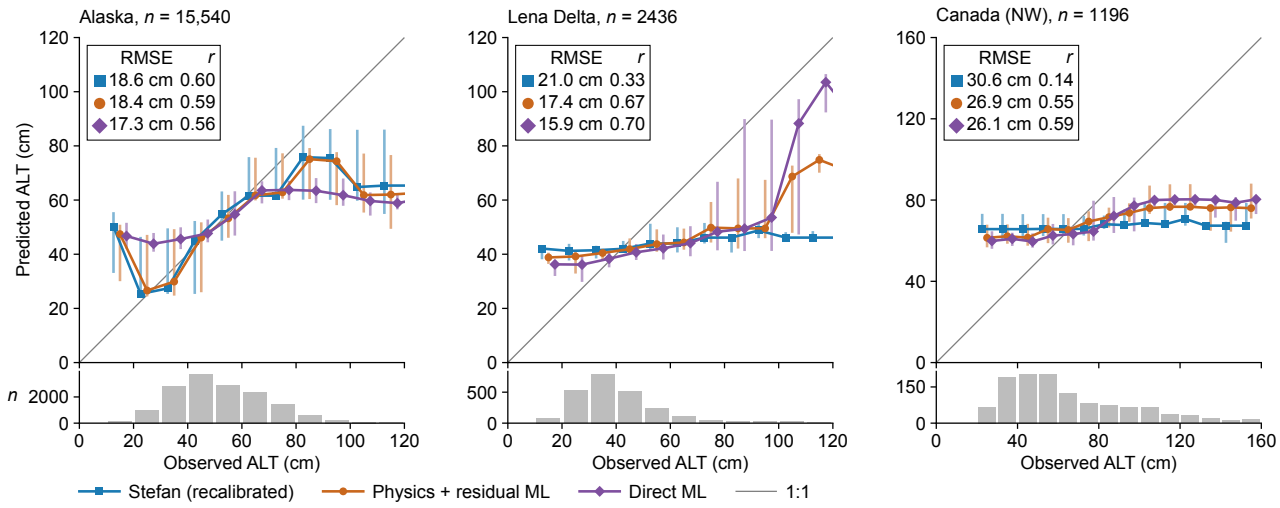

Figure S3. Observed against predicted ALT under spatial-block cross-validation. Median and interquartile range of the predictions per 10 cm bin of observed ALT.

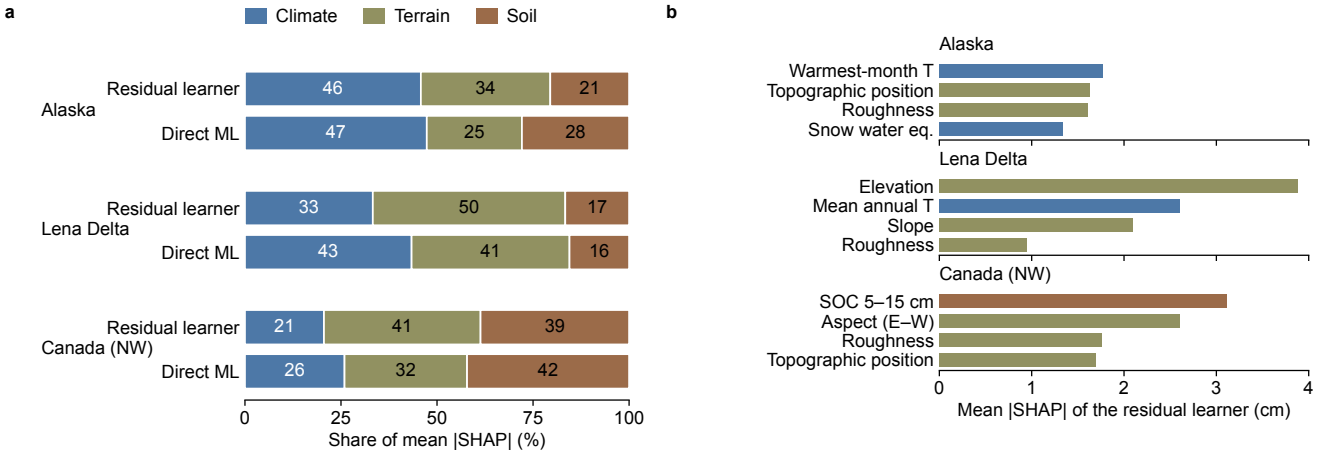

Figure S4. Contribution of the inputs to the residual and direct models. Mean absolute SHAP value by input group (a) and the four largest inputs of the residual model (b).

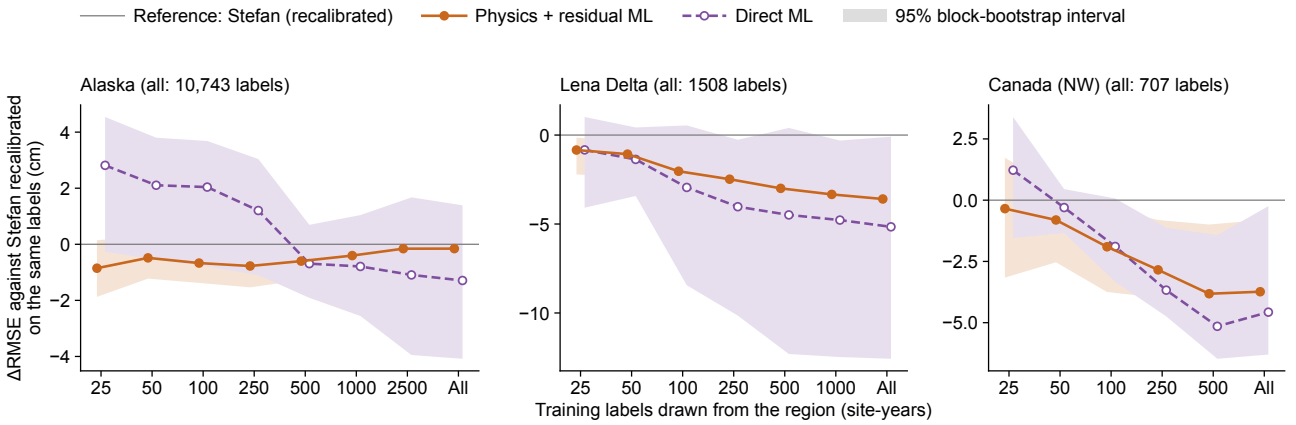

Figure S5. RMSE against the number of labels within a region. Difference from a Stefan model recalibrated on the same labels; bands, 95% block-bootstrap intervals.

Table S6. RMSE and mean bias (cm) on the common site-years. >25 km, site-years more than 25 km from the training sites of Wei et al.

Series	RMSE, all	RMSE, >25 km	Bias, all
Alaska (n = 14,326 / 4229)			
Physics + residual ML	17.1	15.3	−2.9
Stefan, recalibrated	17.4	15.3	−2.1
Wei et al. 2026	17.9	20.8	+3.9
Liu et al. 2024	18.8	15.2	+5.7
ESA CCI v4	27.1	20.1	−2.8
ESA CCI v5	67.6	118.5	+30.5
Aalto et al. 2018	46.2	63.5	−7.5
Lena Delta (n = 461 / 449)			
Physics + residual ML	21.1	21.2	+2.8
Stefan, recalibrated	25.5	25.6	+5.7
Wei et al. 2026	34.6	34.8	+21.9
Liu et al. 2024	33.0	33.2	+19.8
ESA CCI v4	31.0	30.9	−4.7
ESA CCI v5	28.4	28.4	+1.3
Aalto et al. 2018	30.6	30.8	+16.7
Canada (NW) (n = 532 / 489)			
Physics + residual ML	25.8	23.6	+3.4
Stefan, recalibrated	29.6	27.4	+6.1
Wei et al. 2026	27.0	27.4	+10.6
Liu et al. 2024	27.9	28.8	+16.3
ESA CCI v4	33.5	27.9	−7.2
ESA CCI v5	76.0	74.3	+42.8
Aalto et al. 2018	56.5	55.7	+3.9

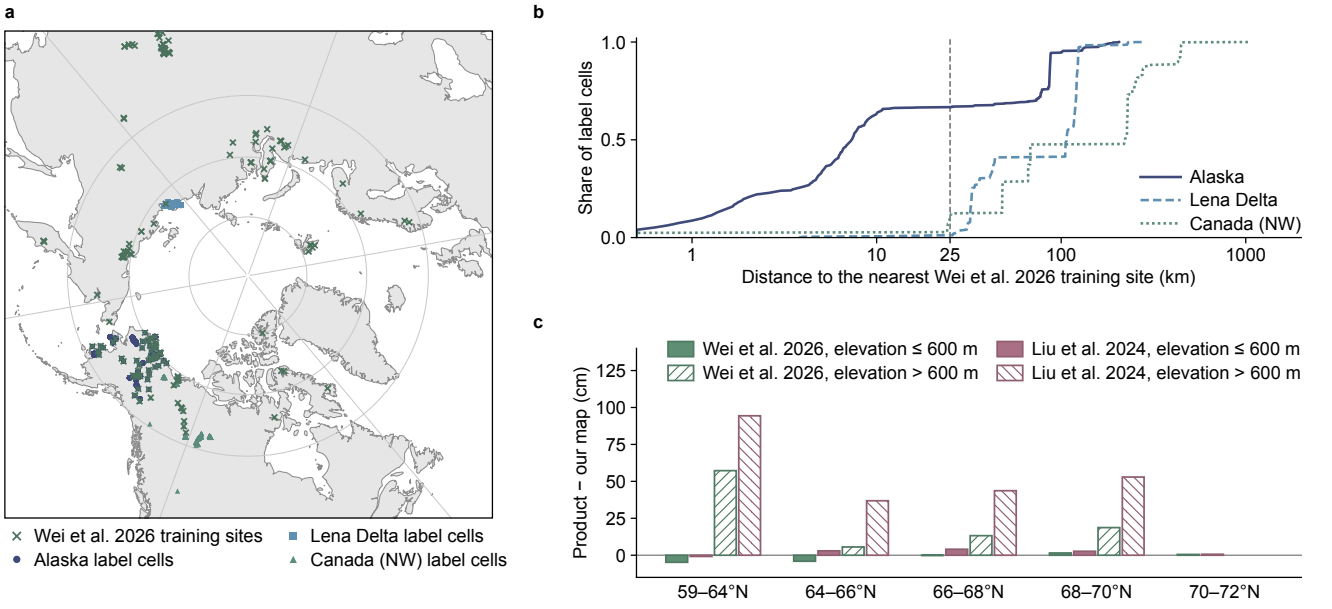

Figure S6. Training sites of Wei et al. and differences between the maps. (a) Training sites and label cells. (b) Distance from the label cells to the nearest training site. (c) Mean difference between the products and our Alaska map of 2013 by latitude, below and above 600 m.

RMSE (cm) per observation year on the site-years with a Wei et al. value; Liu et al. on its subset (to 2020)

Alaska

Year	*n*	Stefan (recal.)	Physics + ML	Wei 2026	Liu 2024
2010	60	18.2	15.3	7.9	13.5
2011	56	16.2	14.9	8.1	13.9
2012	55	18.3	16.5	10.1	11.8
2013	1343	17.2	16.7	15.9	15.0
2014	7861	15.6	15.5	15.5	18.4
2015	171	24.8	21.9	17.8	16.4
2016	2237	16.2	16.0	18.2	15.6
2017	877	21.5	20.1	20.0	20.0
2018	1526	19.3	18.3	19.9	20.8
2019	450	26.7	27.7	28.2	28.3
2020	149	33.8	36.6	45.6	41.7
2021	323	36.6	38.4	46.0	–
2022	369	30.2	31.1	34.8	–

Lena Delta

Year	*n*	Stefan (recal.)	Physics + ML	Wei 2026	Liu 2024
2013	144	22.3	19.8	39.5	40.4
2014	75	11.4	10.4	20.5	19.3
2015	217	8.2	6.8	23.4	17.2
2016	162	14.0	9.7	25.1	25.7
2017	109	12.5	11.3	18.3	–
2020	38	75.7	62.9	69.4	–

Canada (NW)

Year	*n*	Stefan (recal.)	Physics + ML	Wei 2026	Liu 2024
2013	120	20.7	20.9	29.7	18.3
2017	150	30.1	24.3	21.4	30.1
2018	150	26.2	21.1	25.6	32.1
2019	65	35.9	32.5	36.2	31.2
2021	44	25.1	22.0	16.7	–
2022	445	25.2	23.1	26.5	–
2023	80	42.2	35.6	38.2	–
2024	80	49.9	42.6	27.0	–

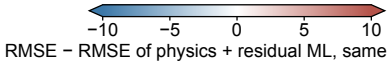

Figure S7. RMSE per observation year (years with at least 30 site-years). Colour, difference from the physics-residual model of the same year.

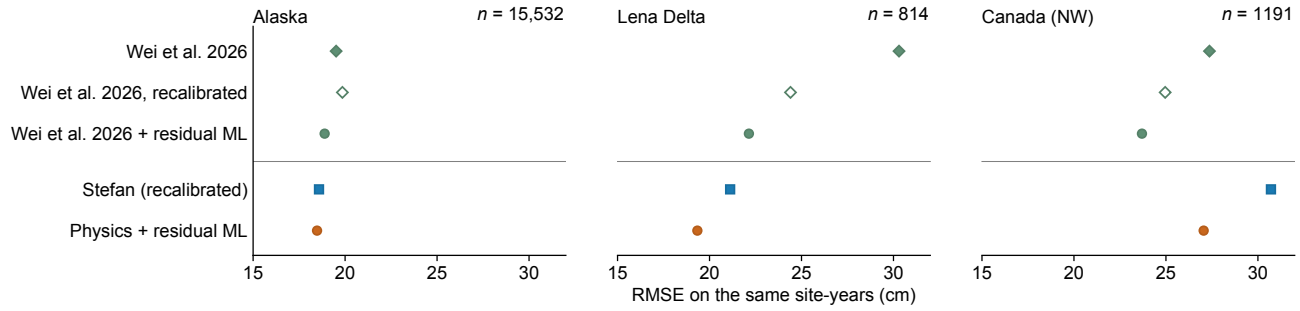

Figure S8. Product-anchored and Stefan-anchored residual learning. Spatial-block RMSE on the site-years with a value of Wei et al.

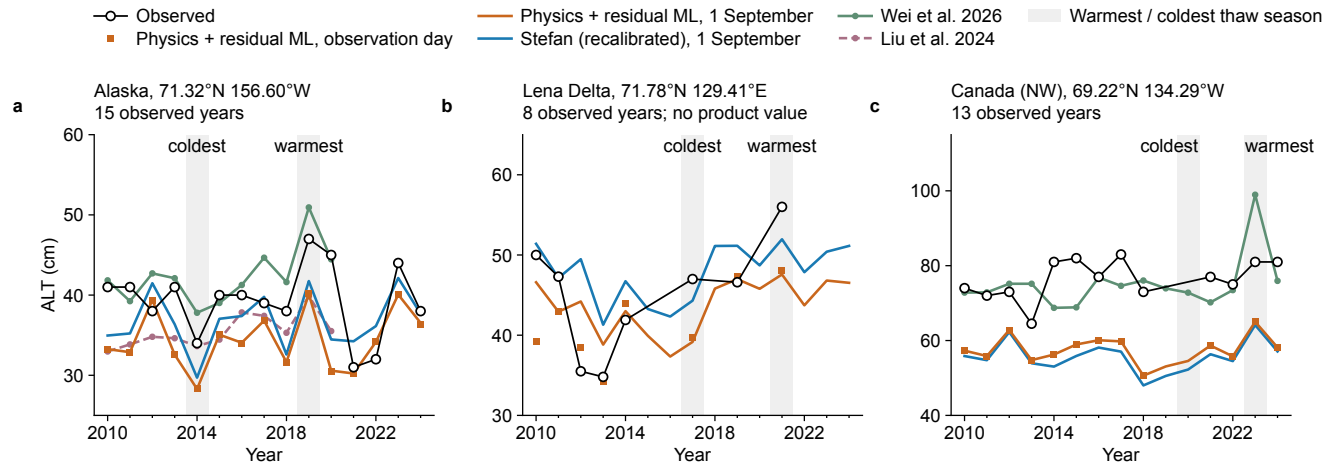

Figure S9. Yearly series at the site with the most observed years in each region. Shading, warmest and coldest thaw seasons.

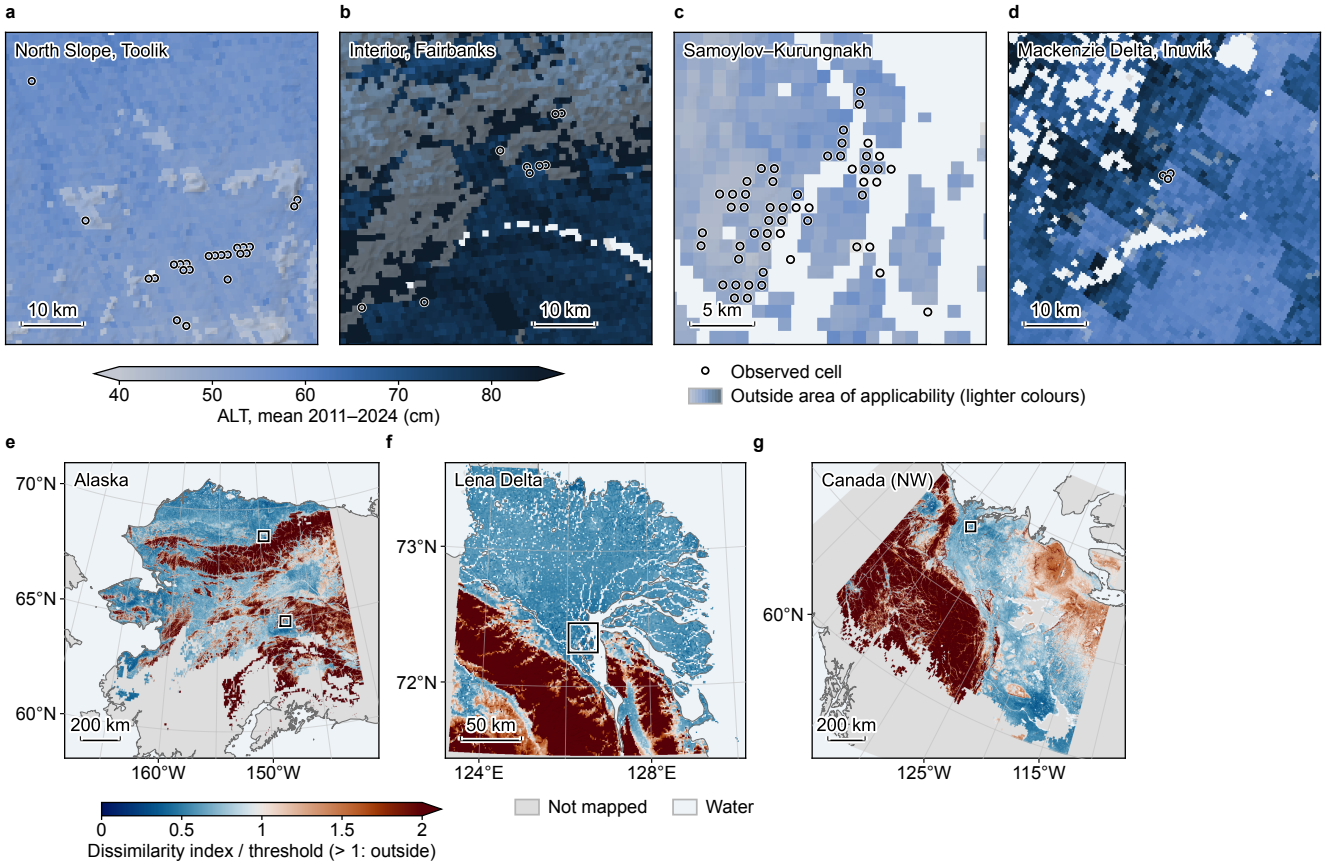

Figure S10. Detail of the 1 km maps and area of applicability. (a–d) Mean ALT of 2011–2024 near Toolik, Fairbanks, Samoylov and the Mackenzie Delta. (e–g) Dissimilarity index relative to the threshold of the area of applicability (above 1, outside).

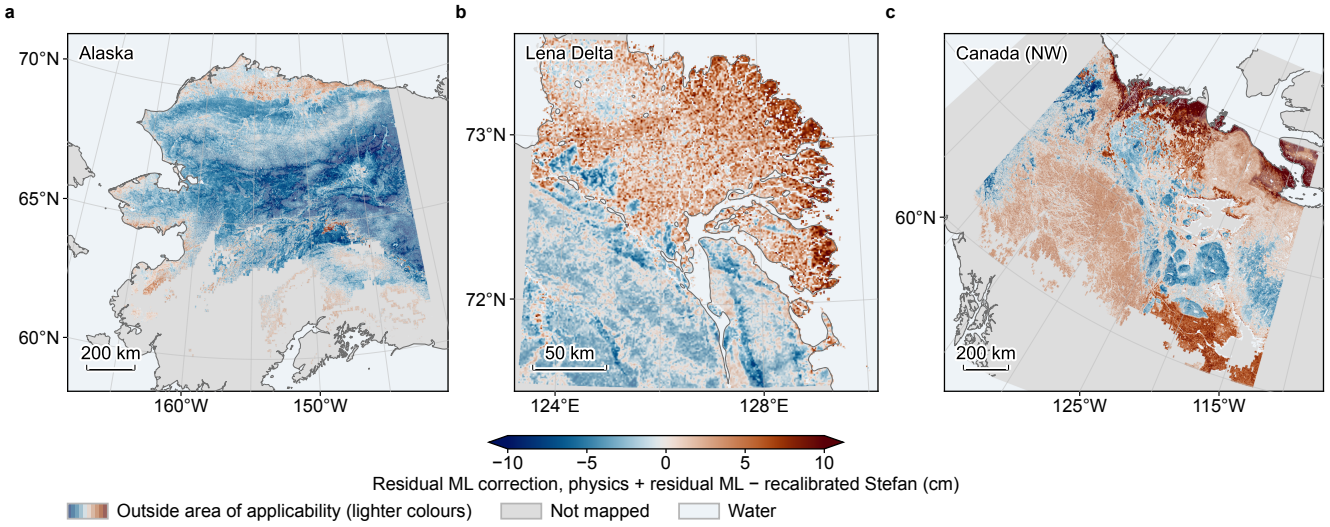

Figure S11. Residual correction of the Stefan model. Physics-residual minus recalibrated Stefan prediction, mean of 2011–2024.

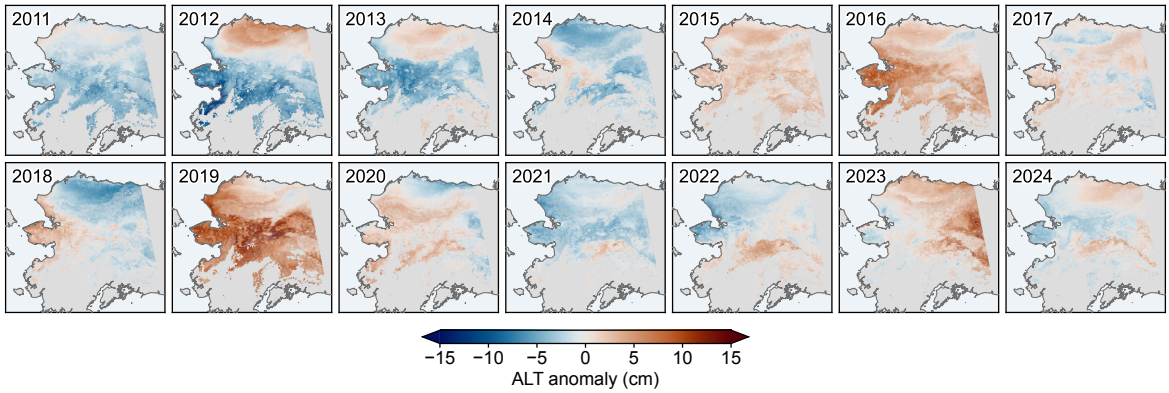

Figure S12. Yearly ALT anomalies in Alaska. Difference from the 2011–2024 mean.

Table S7. RMSE and mean bias (cm) by observation programme under spatial-block cross-validation.

Region	Programme	Protocol	*n*	Mean ALT (cm)	Stefan (recalibrated)	Physics + residual ML	Direct ML
Alaska	ABoVE	probe and GPR transects	14,929	53.4	18.1 / −2.6	18.0 / −3.5	16.7 / +0.5
Alaska	CALM	CALM grid means	611	58.7	27.1 / +2.8	27.2 / +0.1	28.2 / −4.5
Lena Delta	ALLena	probe transects	2436	41.9	21.0 / +1.1	17.4 / +0.5	15.9 / −0.2
Canada (NW)	ABoVE	probe transects	1131	63.4	29.6 / +4.6	25.8 / +3.8	25.3 / +2.6
Canada (NW)	CALM	CALM grid means	65	89.1	44.4 / −26.1	41.0 / −23.0	37.0 / −20.5

References

1. Moore, M. A. *et al.* ABoVE: soil moisture and active layer thickness in Alaska, USA and Canada, 2005–2024, version 2. *ORNL Distributed Active Archive Center* https://doi.org/10.3334/ORNLDAAC/2369 (2025).
2. Streletskiy, D. A. *et al.* GTN-P CALM: 35 years of active layer thickness (ALT) across latitudinal and elevational gradients in the Northern Hemisphere. *PANGAEA* https://doi.org/10.1594/PANGAEA.972777 (2025).
3. Veremeeva, A. *et al.* ALLena: thaw depth measurements of the active layer in the Lena River Delta region from 1998 to 2022, Northeastern Siberia. *PANGAEA* https://doi.org/10.1594/PANGAEA.973813 (2025).
4. Wei, Y., Wu, Z., Wang, J., Shen, H. & Chen, Y. A 1 km resolution dataset of Northern Hemisphere permafrost active layer thickness (2000–2024). Preprint at https://doi.org/10.5194/essd-2026-447 (2026).
5. Liu, Z. *et al.* Widespread deepening of the active layer in northern permafrost regions from 2003 to 2020. *Environ. Res. Lett.* **19**, 014020 (2024). DOI 10.1088/1748-9326/ad0f73.
6. Westermann, S. *et al.* ESA Permafrost Climate Change Initiative (Permafrost_cci): permafrost active layer thickness for the Northern Hemisphere, v4.0. *NERC EDS Centre for Environmental Data Analysis* https://doi.org/10.5285/d34330ce3f604e368c06d76de1987ce5 (2024).
7. Westermann, S. *et al.* ESA Permafrost Climate Change Initiative (Permafrost_cci): permafrost active layer thickness for the Northern Hemisphere, v5.0. *NERC EDS Centre for Environmental Data Analysis* https://doi.org/10.5285/a6fbedd8ee5b472c8e84e55f746c1704 (2025).
8. Aalto, J., Karjalainen, O., Hjort, J. & Luoto, M. Statistical forecasting of current and future circum-Arctic ground temperatures and active layer thickness. *Geophys. Res. Lett.* **45**, 4889–4898 (2018). DOI 10.1029/2018GL078007.
9. Yi, Y. & Kimball, J. S. ABoVE: active layer thickness from remote sensing permafrost model, Alaska, 2001–2015. *ORNL Distributed Active Archive Center* https://doi.org/10.3334/ORNLDAAC/1760 (2020).
10. Lundberg, S. M. & Lee, S.-I. A unified approach to interpreting model predictions. *Adv. Neural Inf. Process. Syst.* **30**, 4765–4774 (2017).
11. Muñoz-Sabater, J. *et al.* ERA5-Land: a state-of-the-art global reanalysis dataset for land applications. *Earth Syst. Sci. Data* **13**, 4349–4383 (2021). DOI 10.5194/essd-13-4349-2021.
12. Copernicus Climate Change Service. ERA5-Land monthly averaged data from 1950 to present. *Copernicus Climate Change Service (C3S) Climate Data Store (CDS)* https://doi.org/10.24381/cds.68d2bb30 (2019).
13. European Space Agency & Airbus. Copernicus DEM. *European Space Agency* https://doi.org/10.5270/ESA-c5d3d65 (2022).
14. Poggio, L. *et al.* SoilGrids 2.0: producing soil information for the globe with quantified spatial uncertainty. *SOIL* **7**, 217–240 (2021). DOI 10.5194/soil-7-217-2021.
15. Didan, K. MODIS/Terra vegetation indices 16-day L3 global 250m SIN grid V061. *NASA EOSDIS Land Processes DAAC* https://doi.org/10.5067/MODIS/MOD13Q1.061 (2021).
16. Hall, D. K. & Riggs, G. A. MODIS/Terra snow cover 8-day L3 global 500m SIN grid, version 61. *NASA National Snow and Ice Data Center DAAC* https://doi.org/10.5067/MODIS/MOD10A2.061 (2021).
17. Pekel, J.-F., Cottam, A., Gorelick, N. & Belward, A. S. High-resolution mapping of global surface water and its long-term changes. *Nature* **540**, 418–422 (2016). DOI 10.1038/nature20584.
18. Hugelius, G. *et al.* The Northern Circumpolar Soil Carbon Database: spatially distributed datasets of soil coverage and soil carbon storage in the northern permafrost regions. *Earth Syst. Sci. Data* **5**, 3–13 (2013). DOI 10.5194/essd-5-3-2013.
19. Hugelius, G. *et al.* A new data set for estimating organic carbon storage to 3 m depth in soils of the northern circumpolar permafrost region. *Earth Syst. Sci. Data* **5**, 393–402 (2013). DOI 10.5194/essd-5-393-2013.
20. Raynolds, M. K. *et al.* A raster version of the Circumpolar Arctic Vegetation Map (CAVM). *Remote Sens. Environ.* **232**, 111297 (2019). DOI 10.1016/j.rse.2019.111297.
21. Zanaga, D. *et al.* ESA WorldCover 10 m 2021 v200. *Zenodo* https://doi.org/10.5281/zenodo.7254221 (2022).
22. Westermann, S. *et al.* ESA Permafrost Climate Change Initiative (Permafrost_cci): permafrost extent for the Northern Hemisphere, v4.0. *NERC EDS Centre for Environmental Data Analysis* https://doi.org/10.5285/93444bc1c4364a59869e004bf9bfd94a (2024).

23. Wei, Y. & Chen, Y. A 1 km resolution dataset of Northern Hemisphere permafrost active layer thickness (2000–2024), version 2. *Zenodo* https://doi.org/10.5281/zenodo.21667583 (2026).

24. Liu, Z. Gridded active layer thickness across northern permafrost regions from 2003 to 2020. *Zenodo* https://doi.org/10.5281/zenodo.10070610 (2023).

25. Aalto, J., Karjalainen, O., Hjort, J. & Luoto, M. Data from: statistical forecasting of current and future circum-Arctic ground temperatures and active layer thickness. *Dryad* https://doi.org/10.5061/dryad.886pr72 (2019).